Biotechnol Lett (2015) 37:317–326
DOI 10.1007/s10529-014-1696-x

ERRATUM

Erratum to: A coupled thermodynamic and metabolic control analysis methodology and its evaluation on glycerol biosynthesis in *Saccharomyces cerevisiae*

Markus Birkenmeier · Matthias Mack · Thorsten Röder

Published online: 29 October 2014

Abstract A coupled *in silico* thermodynamic and probabilistic metabolic control analysis methodology was verified by applying it to the glycerol biosynthetic pathway in *Saccharomyces cerevisiae*. The methodology allows predictions even when detailed knowledge of the enzyme kinetics is lacking. In a metabolic steady state, we found that glycerol-3-phosphate dehydrogenase operates far from thermodynamic equilibrium ($\Delta_r G'_1$ −15.9 to −47.5 kJ mol^{-1}, where $\Delta_r G'_1$ is the transformed Gibbs energy of the reaction). Glycerol-3-phosphatase operates in modes near the thermodynamic equilibrium, far from the thermodynamic equilibrium or in between ($\Delta_r G'_2 \approx 0$ to −23.7 kJ mol^{-1}). From the calculated distribution of the scaled flux control coefficients (median = 0.81), we inferred that the pathway flux is primarily controlled by glycerol-3-phosphate dehydrogenase. This prediction is consistent with previous findings, verifying the efficacy of the proposed methodology.

Keywords Glycerol biosynthesis · Metabolic control analysis · Random sampling · *Saccharomyces cerevisiae* · Thermodynamic analysis · Uncertainty modeling

List of symbols

$\mathbf{\Delta_r G'}$	Vector of transformed Gibbs energies of reaction
$\Delta_r G'_1$	Transformed Gibbs energy of glycerol-3-phosphate dehydrogenase reaction (reaction 1)
$\Delta_r G'_2$	Transformed Gibbs energy of glycerol-3-phosphatase reaction (reaction 2)
$\Delta_r G'^0_1$	Standard transformed Gibbs energy of glycerol-3-phosphate dehydrogenase reaction (reaction 1)

Electronic supplementary material The online version of this article (doi:10.1007/s10529-014-1696-x) contains supplementary material, which is available to authorized users.

Erratum to: Biotechnol Lett. doi:10.1007/s10529-014-1675-2
Unfortunately, in the original publication of the article some errors occurred in both text and formulas during the typesetting process. Hence the correct version of the article is published as an erratum.

The online version of the original article can be found under doi:10.1007/s10529-014-1675-2.

M. Birkenmeier · T. Röder (✉)
Institute for Chemical Process Engineering, Mannheim University of Applied Sciences, Paul-Wittsack-Straße 10, 68163 Mannheim, Germany
e-mail: t.roeder@hs-mannheim.de

M. Birkenmeier
e-mail: m.birkenmeier@hs-mannheim.de

M. Mack
Institute for Technical Microbiology, Mannheim University of Applied Sciences, Paul-Wittsack-Straße 10, 68163 Mannheim, Germany
e-mail: m.mack@hs-mannheim.de

$\Delta_r G_2'^0$ Standard transformed Gibbs energy of glycerol-3-phosphatase reaction (reaction 2)
$\mathbf{\Delta_r G'^0}$ Vector of standard transformed Gibbs energies of reaction
R Universal gas constant
T Temperature
$\mathbf{N^T}$ Transposed stoichiometric matrix in the thermodynamic analysis
$\mathbf{c}$ Vector of metabolite concentrations
$\mathbf{c}_{\min}$ Vector of minimum metabolite concentrations
$\mathbf{c}_{\max}$ Vector of maximum metabolite concentrations
$[G3P]$ Glycerol-3-phosphate concentration
$\boldsymbol{\rho}$ Vector of disequilibrium ratios
ρ_1 Disequilibrium ratio of glycerol-3-phosphate dehydrogenase reaction (reaction 1)
ρ_2 Disequilibrium ratio of glycerol-3-phosphatase reaction (reaction 2)
$\mathbf{V}$ Diagonal matrix of steady-state fluxes
$\mathbf{v}$ Vector of steady-state fluxes
v_{net} Steady-state net flux of the pathway
$v_{net,1}$ Steady-state net flux of glycerol-3-phosphate dehydrogenase (reaction 1)
$v_{net,2}$ Steady-state net flux of glycerol-3-phosphatase (reaction 2)
$v_{+,1}$ Forward steady-state flux of glycerol-3-phosphate dehydrogenase (reaction 1)
$v_{-,1}$ Backward steady-state flux of glycerol-3-phosphate dehydrogenase (reaction 1)
$\mathbf{C_e^{G3P}}$ Matrix of scaled concentration control coefficients
$\mathbf{C_e^v}$ Matrix of scaled flux control coefficients
$C_{e_1}^{v_{net}}$ Scaled flux control coefficient of glycerol-3-phosphate dehydrogenase (reaction 1) related to v_{net}
$C_{e_2}^{v_{net}}$ Scaled flux control coefficient of glycerol-3-phosphatase (reaction 2) related to v_{net}
$\mathbf{e}$ Vector of enzyme concentrations
e_1 Enzyme concentration of glycerol-3-phosphate dehydrogenase (reaction 1)
e_2 Enzyme concentration of glycerol-3-phosphatase (reaction 2)
$\mathbf{E_{G3P}^v}$ Matrix of scaled elasticities: local sensitivities of $\mathbf{v}$ to changes in $[G3P]$
$E_{G3P}^{v_{+,1}}$ Scaled elasticity: sensitivity of $v_{+,1}$ to changes in $[G3P]$
$E_{G3P}^{v_{-,1}}$ Scaled elasticity: sensitivity of $v_{-,1}$ to changes in $[G3P]$
$\mathbf{\Pi_e^v}$ Matrix of scaled elasticities: local sensitivities of $\mathbf{v}$ to changes in $\mathbf{e}$
$\mathbf{N}_{\text{MCA}}$ Stoichiometric matrix of the metabolic control analysis
$Q_{0.2}$ 20 % quantile
$Q_{0.8}$ 80 % quantile

Introduction

To compensate for the lack of *in vivo* kinetic enzyme data, researchers use probabilistic modeling approaches to predict the properties of metabolic networks (Klipp et al. 2004; Wang et al. 2004; Steuer et al. 2006; Tran et al. 2008; Murabito et al. 2011). These approaches are based on randomized sampling of unknown or uncertain parameters within a constrained parameter space (Murabito et al. 2011; Murabito 2013). One such approach is the ORACLE (Optimization and Risk Analysis of Complex Living Entities) framework developed by Hatzimanikatis and coworkers (Wang et al. 2004; Miskovic and Hatzimanikatis 2010; Soh et al. 2012; Chakrabarti et al. 2013). This framework samples enzyme elasticities and integrates thermodynamic and other data sources into a probabilistic metabolic control analysis (MCA) of metabolic networks (Soh et al. 2012).

Inspired by the ORACLE framework, we performed a thermodynamic and metabolic control analysis of the glycerol biosynthetic pathway in *Saccharomyces cerevisiae*. This pathway is of special interest to the bioethanol production industry (He et al. 2014), because high rates of glycerol formation decrease the practical ethanol yields in current fermentation processes (Hubmann et al. 2011). Since data on the glycerol biosynthetic pathway are widely available, we selected this pathway as a model for verifying our proposed approach. Nevertheless, to form a better understanding of the thermodynamic and control properties of this pathway, an additional mathematical analysis should be conducted. Therefore, we calculated thermodynamically feasible transformed Gibbs energies of the relevant reactions, and obtained the disequilibrium ratios. Similar to the ORACLE methodology, the disequilibrium ratios are

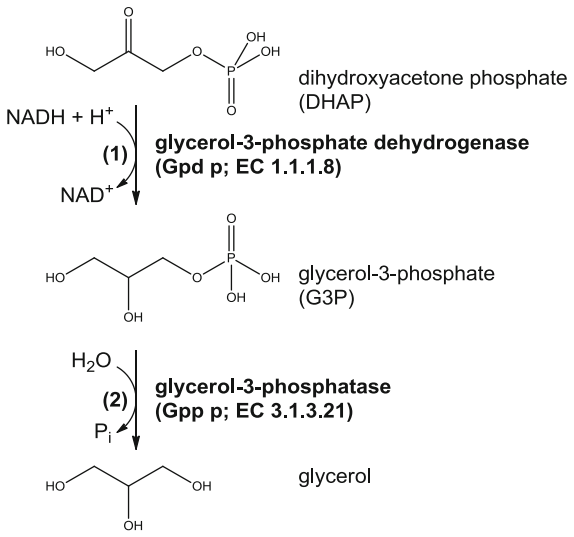

Fig. 1 Reaction scheme of the glycerol biosynthesis pathway in *Saccharomyces cerevisiae* (derived from Cronwright et al. 2002)

input to the probabilistic MCA. The MCA procedure assumes no specific knowledge of the enzyme kinetic rate laws. The aim of the study was to evaluate the capability of the methodology and to examine the influence of the enzyme kinetics on the flux control coefficients. Finally, to verify the methodology, we compared the calculated distributions of the flux control coefficients with coefficients reported in the literature.

Methods

Metabolic pathway

Figure 1 depicts the essential reactions in the glycerol biosynthetic pathway. The precursor dihydroxyacetone phosphate (DHAP), an intermediate of glycolysis, is converted in a two-step reaction cascade to glycerol in the cytosol of *Saccharomyces cerevisiae* (He et al. 2014). The first reaction, the conversion of DHAP to glycerol-3-phosphate (G3P), is catalyzed by NADH-dependent glycerol-3-phosphate dehydrogenase (Gpd p, reaction 1). In the second reaction, glycerol-3-phosphatase (Gpp p, reaction 2) catalyzes the conversion of G3P to glycerol (Cronwright et al. 2002).

Thermodynamic analysis

The proposed thermodynamic analysis is based on the second law of thermodynamics. This law states that any chemical reaction occurs in the direction of negative Gibbs energy. Furthermore, this constraint simultaneously holds for every reaction in a metabolic network under non-equilibrium steady-state conditions (Kümmel et al. 2006; Cvijovic et al. 2011). In a biochemical thermodynamics context, this constraint is expressed as

$$\mathbf{\Delta_r G'} < \mathbf{0} \tag{1}$$

In metabolic reaction networks, $\mathbf{\Delta_r G'}$ denotes the vector of the transformed Gibbs energies of the reactions in the network. At constant temperature and pressure, $\mathbf{\Delta_r G'}$ is given by

$$\mathbf{\Delta_r G'} = \mathbf{\Delta_r G'^0} + R \cdot T \cdot \mathbf{N^T} \cdot \ln(\mathbf{c}) \tag{2}$$

where $\mathbf{\Delta_r G'^0}$ represents the vector of the standard transformed Gibbs energies of the reactions, R is the universal gas constant, T is the temperature, $\mathbf{c}$ is the vector of metabolite concentrations and $\mathbf{N^T}$ is the transposed stoichiometric matrix containing the stoichiometric coefficients of the metabolites. Equation (2) assumes that the cytosol is a dilute aqueous solution (Alberty et al. 2011). Kümmel et al. (2006) adopted Eq. (2) into a constrained optimization procedure called NET analysis (Network-Embedded Thermodynamic analysis). Using this approach, we calculated the ranges of the two transformed Gibbs energies of reaction in this metabolic pathway ($\Delta_r G'_1$ for reaction 1 and $\Delta_r G'_2$ for reaction 2 in $\mathbf{\Delta_r G'}$). The ranges are determined by maximizing and minimizing the transformed Gibbs energies of reactions under the constraint of Eq. (1) (assuming a positive net flux in the direction of dihydroxyacetone phosphate to glycerol). For this purpose, the metabolite concentrations are constrained within the range

$$\mathbf{c_{min}} \leq \mathbf{c} \leq \mathbf{c_{max}} \tag{3}$$

where $\mathbf{c_{min}}$ and $\mathbf{c_{max}}$ are the vectors of minimum and maximum metabolite concentrations, respectively [see Eq. (2); the metabolite concentrations are variables in the optimization procedure].

The metabolite concentration ranges in the present study were mainly derived from intracellular

concentrations measured by Cronwright et al. (2002) (for details, see Supporting Information). To determine the standard transformed Gibbs energy of reaction of glycerol-3-phosphate dehydrogenase $\Delta_r G_1'^0$ and glycerol-3-phosphatase $\Delta_r G_2'^0$ (in $\mathbf{\Delta_r G'^0}$ of Eq. (2)), we used data listed in Goldberg et al. (1993) (based on Young and Pace (1958)) and Goldberg and Tewari (1994) (based on Romero and de Meis (1989)), respectively. From these data, $\Delta_r G_1'^0$ and $\Delta_r G_2'^0$ were calculated as -26.5 and -10.8 kJ mol^{-1}, respectively, at pH 7 and 308.15 K (details are provided in the Supporting Information).

Thermodynamically feasible pathway states [combinations of $\Delta_r G_1'$ and $\Delta_r G_2'$ in $\mathbf{\Delta_r G'}$ fulfilling Eq. (1)] were generated by sampling the metabolite concentrations within their constrained logarithmic space, as described by Chakrabarti et al. (2013). The sampling was conducted by the Artificial-Centering Hit-and-Run sampler within the MATLAB function *cprnd*, programmed by Benham (2011) and based on Kaufman and Smith (1998) (see Supporting Information for details).

The thermodynamically feasible combinations of $\Delta_r G_1'$ and $\Delta_r G_2'$ were converted to combinations of disequilibrium ratios ρ_1 and ρ_2 by the following equation (shown for $\Delta_r G_1'$):

$$\rho_1 = \exp\left(\frac{\Delta_r G_1'}{R \cdot T}\right) = \frac{v_{-,1}}{v_{+,1}} \tag{4}$$

The disequilibrium ratio is the ratio of backward to forward steady-state reaction fluxes (in reaction 1, the backward and forward fluxes are denoted by $v_{-,1}$ and $v_{+,1}$, respectively) (Rolleston 1972; Fell 1997). At thermodynamic equilibrium the disequilibrium ratio equals one; in the forward and reverse reaction directions, it is less than or greater than one, respectively (Soh and Hatzimanikatis 2010). Furthermore, the backward and forward steady-state fluxes can be calculated from the given steady-state net flux and the disequilibrium ratio (Fell 1997). Specifically, in reaction 1 we have

$$v_{+,1} = \frac{v_{net}}{1-\rho_1} \text{ and } v_{-,1} = v_{+,1} - v_{net,} \tag{5}$$

where v_{net} is the steady-state net flux in the glycerol biosynthetic pathway (which is positive in the dihydroxyacetone phosphate-to-glycerol direction). In steady state, the net fluxes of reaction 1 $(v_{net,1})$ and reaction 2 $(v_{net,2})$ are equal and both are denoted as v_{net}.

In addition, Eq. (5) indicates that the calculated disequilibrium ratios are suitable input parameters to a probabilistic metabolic control analysis (Wang et al. 2004).

Metabolic control analysis

Metabolic control analysis (MCA) theory, introduced by Kacser and Burns (1973) and Heinrich and Rapoport (1974), is based on the (scaled) concentration and (scaled) flux control coefficients. In the present study, the steady-state glycerol-3-phosphate (G3P) concentration and the steady-state fluxes, $\mathbf{v}$, respond to infinitesimal changes in the enzyme concentrations $\mathbf{e}$ (Wang et al. 2004; Murabito et al. 2011). These responses are described by the scaled concentration control coefficients, $\mathbf{C_e^{G3P}}$, and the scaled flux control coefficients, $\mathbf{C_e^v}$, respectively, given by (in matrix notation):

$$\mathbf{C_e^{G3P}} = \frac{\partial \ln([G3P])}{\partial \ln(\mathbf{e})} \tag{6}$$

$$\mathbf{C_e^v} = \frac{\partial \ln(\mathbf{v})}{\partial \ln(\mathbf{e})} \tag{7}$$

In the log–linear formulation, the control coefficient matrices are evaluated as (Reder 1988; Hatzimanikatis et al. 1996; Wang et al. 2004):

$$\mathbf{C_e^{G3P}} = -\left(\mathbf{N_{MCA}} \cdot \mathbf{V}(\boldsymbol{\rho}, v_{net}) \cdot \mathbf{E_{G3P}^v}\right)^{-1} \cdot \mathbf{N_{MCA}} \cdot \mathbf{V}(\boldsymbol{\rho}, v_{net}) \cdot \mathbf{\Pi_e^v} \tag{8}$$

$$\mathbf{C_e^v} = \mathbf{E_{G3P}^v} \cdot \mathbf{C_e^{G3P}} + \mathbf{\Pi_e^v} \tag{9}$$

where $\mathbf{N_{MCA}}$ denotes the stoichiometric matrix derived from the model of Cronwright et al. (2002). $\mathbf{N_{MCA}}$ is a one-row four-column matrix containing the stoichiometric coefficients for G3P. Here, the two net fluxes are split into forward and backward fluxes. $\mathbf{V}(\boldsymbol{\rho}, v_{net})$ is a diagonal 4×4 matrix of steady state fluxes, in which the backward and forward fluxes are calculated from a given steady-state net flux v_{net} and a combination of disequilibrium ratios (ρ_1 and ρ_2 within $\boldsymbol{\rho}$). $\mathbf{E_{G3P}^V}$ is a 4×1 matrix of scaled elasticities with respect to the G3P concentration ($\mathbf{E_{G3P}^v} = \partial \ln(\mathbf{v}) / \partial \ln([G3P])$), denoting the local sensitivities

of the fluxes **v** to the G3P concentration, and $\Pi_{\mathbf{e}}^{\mathbf{v}}$ is a 4 × 2 matrix of scaled elasticities with respect to the enzyme concentrations **e** ($\Pi_{\mathbf{e}}^{\mathbf{v}} = \partial \ln(\mathbf{v})/\partial \ln(\mathbf{e})$), denoting the local sensitivities of the fluxes **v** to the enzyme concentrations **e**. Since enzyme reaction rates are typically proportional to the enzyme concentrations, the scaled elasticities in $\Pi_{\mathbf{e}}^{\mathbf{v}}$ are equal to one (Wang et al. 2004).

In this study, the scaled flux control coefficients are calculated similarly to those of Wang et al. (2004). Our MCA study is based on the model of Cronwright et al. (2002), but adopts different approaches for describing the enzyme kinetics within the MCA procedure.

To calculate the distributions of scaled flux control coefficients, we generated thermodynamically feasible combinations of disequilibrium ratios in $\boldsymbol{\rho}$, specified the steady-state net flux v_{net} and generated the scaled elasticity values in $\mathbf{E}_{\mathbf{G3P}}^{\mathbf{v}}$. The scaled elasticities in $\mathbf{E}_{\mathbf{G3P}}^{\mathbf{v}}$ were generated by two sampling approaches. In case (i), we uniformly sampled the scaled elasticities within defined ranges, and correlated the scaled elasticities of the forward and backward fluxes in the same reaction (e.g. $E_{G3P}^{v_{+,1}}$ and $E_{G3P}^{v_{-,1}}$; for further details, see Supporting Information, Steuer et al. (2006) and Grimbs et al. (2007)). In case (ii), we uniformly sampled the degrees of saturation of active sites and calculated the scaled metabolite concentrations as proposed by Wang et al. (2004). In case (ii), two enzyme kinetic rate laws, based on the convenience rate law of Liebermeister and Klipp (2006), were used to derive expressions for the scaled elasticity calculations (Chakrabarti et al. 2013). These expressions depend on the calculated scaled metabolite concentrations (see Supporting Information for details).

For each of the two cases described above, we computed 4×10^6 stable steady states and their corresponding scaled flux control coefficients related to v_{net} (for details, see Supporting Information). The local stability of the states was checked by calculating the eigenvalue of the Jacobian matrix of the system. In general, the stability criterion is that all eigenvalues of the Jacobian have negative real parts. The obtained distributions of the scaled flux control coefficients were also statistically evaluated to examine the flux control trend (Wang et al. 2004; Miskovic and Hatzimanikatis 2010).

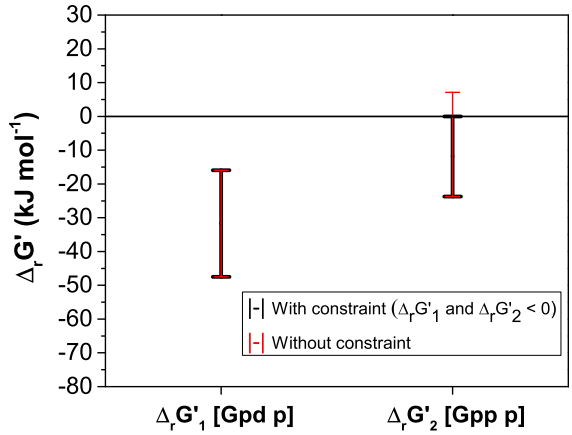

Fig. 2 Calculated ranges of $\Delta_r G'_1$ and $\Delta_r G'_2$, evaluated by an optimization procedure at pH 7 and 308.15 K. *Thick black bars* indicate the thermodynamically feasible ranges in a metabolic steady state of the pathway (i.e. $\mathbf{\Delta_r G'} < \mathbf{0}$). *Thin red bars* are the ranges calculated without imposing $\mathbf{\Delta_r G'} < \mathbf{0}$; the possible ranges are restricted only by the defined metabolite concentration ranges (metabolite concentration ranges are provided in the Supporting Information)

Results and discussion

Thermodynamic analysis

Figure 2 shows the calculated ranges of the transformed Gibbs energies of reaction $\mathbf{\Delta_r G'}$ for the pathway operating in metabolic steady state [under the constraint of Eq. (1)] and in non-steady-state [unconstrained by Eq. (1)].

Under the investigated conditions, the transformed Gibbs energy of reaction of glycerol-3-phosphate dehydrogenase $\Delta_r G'_1$ (Gpd p, reaction 1) ranges from −15.9 to −47.5 kJ mol^{-1}, in both steady and non-steady states. Hence, glycerol-3-phosphate dehydrogenase is active at all metabolite concentrations investigated in this study far from thermodynamic equilibrium. The reaction strongly favors glycerol-3-phosphate formation and a positive net flux occurs from dihydroxyacetone phosphate to glycerol-3-phosphate. This flux arises from the negative standard transformed Gibbs energy of reaction $\Delta_r G'^0_1$ (−26.5 kJ mol^{-1}), which dominates the $\Delta_r G'_1$ calculation equation. Furthermore, the finding that glycerol-3-phosphate dehydrogenase operates far from thermodynamic equilibrium in *Saccharomyces cerevisiae* is consistent with a study on human cytosolic glycerol-

3-phosphate dehydrogenase (Ou et al. 2006). It has been hypothesized that an enzyme operating far from thermodynamic equilibrium is more likely regulated by the cell (Kümmel et al. 2006). This hypothesis is supported by findings that the glycerol-3-phosphate dehydrogenase of *S. cerevisiae* is inhibited by ATP, ADP and fructose 1,6-bisphosphate (Albertyn et al. 1992).

Glycerol-3-phosphatase (Gpp p, reaction 2) is metabolically active in steady state (positive net flux from glycerol-3-phosphate towards glycerol) near the thermodynamic equilibrium ($\Delta_r G'_2 \approx 0$ but slightly negative), far from thermodynamic equilibrium ($\Delta_r G'_2$ up to -23.7 kJ mol^{-1}) or at modes between these extremes. The different $\Delta_r G'_2$ ranges calculated with and without the constraint of Eq. (1) (thick black and thin red bars, respectively, in Fig. 2) indicate that in metabolic steady state, specific combinations of constrained metabolite concentration values are not allowed to fulfill the constraint of Eq. (1) (e.g. high product concentrations, low reactant concentrations or a combination of both are prohibited).

Figure 3a and 3b are histograms of the 4×10^6 thermodynamically feasible combinations of $\Delta_r G'_1$ and $\Delta_r G'_2$ generated in this analysis. The distributions of the histograms can be described as distorted normally distributed (broader maximum). The shape of the individual distributions of $\mathbf{\Delta_r G'}$ is influenced by the defined ranges of metabolite concentrations. For instance, the distribution of $\Delta_r G'_1$ (Gpd p, reaction 1) is shifted in the negative direction relative to $\Delta_r G'^0_1$ of -26.5 kJ mol^{-1}. This shift occurs because the concentration range of glycerol-3-phosphate is broader and covers more smaller concentrations compared with the ranges of other metabolites participating in this reaction (metabolite concentration ranges and sampling procedure are reported in the Supporting Information). Moreover, the ranges of $\Delta_r G'_1$ (-16.3 to -47.2 kJ mol^{-1}) and $\Delta_r G'_2$ (≈ 0 to -23.6 kJ mol^{-1}) are slightly smaller than those computed by the optimization procedure ($\Delta_r G'_1$ -15.9 to -47.5 kJ mol^{-1}, $\Delta_r G'_2$ $\approx$ 0 to -23.7 kJ mol^{-1}). This mismatch is a limitation of the sampling methodology. The exact minimal and maximal values of $\mathbf{\Delta_r G'}$ are unlikely to be reached by the sampling approach. [Note that the full ranges of the generated values are scarcely visible in Fig. 3a and 3b, because the number of boundary values is very small.] To obtain the minimum and maximum $\mathbf{\Delta_r G'}$, we must randomly sample specific combinations of logarithmic metabolite concentrations. However, our metabolic control analysis (MCA) results did not significantly change when the number of $\Delta_r G'_1$ and $\Delta_r G'_2$ combinations was increased beyond 4×10^6.

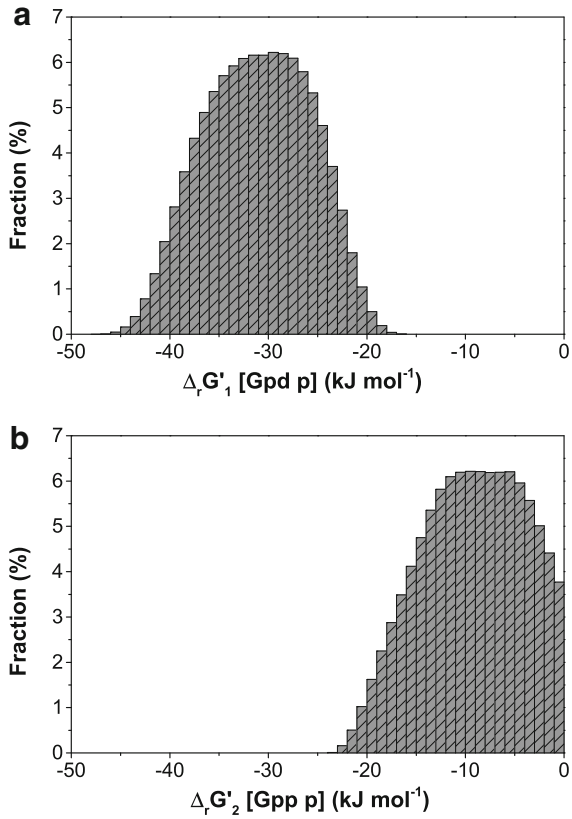

Fig. 3 Histograms showing the distributions of 4×10^6 combinations of thermodynamically feasible $\Delta_r G'_1$ and $\Delta_r G'_2$ values. The combinations were computed by sampling at pH 7 and 308.15 K (details of the sampling methodology are provided in the Supporting Information). **a** histogram of $\Delta_r G'_1$ values. **b** histogram of $\Delta_r G'_2$ values

Subsequently, the generated combinations of $\Delta_r G'_1$ and $\Delta_r G'_2$ were converted to combinations of disequilibrium ratios (ρ_1 and ρ_2) by Eq. (4) (distribution histograms are presented in the Supporting Information). ρ_1 and ρ_2 are the ratios of backward to forward steady-state fluxes of reactions 1 and 2, respectively. The disequilibrium ratio dataset was used to calculate the scaled flux control coefficients (see metabolic control analysis in the Methods section).

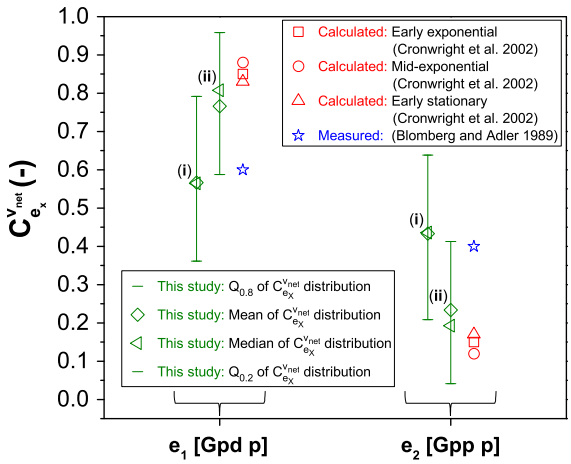

Fig. 4 Statistical parameters of the computed distributions of scaled flux control coefficients (*green diamonds* and *left-pointing triangles* within *bars*). The scaled flux control coefficients extracted from the literature (*red circles*, *squares*, *triangles* and *blue stars*) are shown for comparison. The scaled elasticity values within the metabolic control analysis were generated in two ways: (**i**) correlated uniform sampling of scaled elasticities within defined ranges (Steuer et al. 2006; Grimbs et al. 2007) and (**ii**) uniform sampling of the degrees of saturation of active sites combined with the scaled elasticity expressions derived from two rate laws based on the convenience rate law (Wang et al. 2004; Liebermeister and Klipp 2006; Chakrabarti et al. 2013) (for details, see Supporting Information). In both cases, the 4×10^6 thermodynamically feasible combinations of $\Delta_r G'_1$ and $\Delta_r G'_2$ (converted to ρ_1 and ρ_2) at pH 7 and 308.15 K were used for the generation of 4×10^6 stable steady states, and the corresponding scaled flux control coefficients were determined. The obtained scaled flux control coefficient distributions were statistically evaluated ($Q_{0.2}$: 20 % quantile and $Q_{0.8}$: 80 % quantile)

Metabolic control analysis

Figure 4 shows the statistical parameters of the computed distributions of the scaled flux control coefficients, together with scaled flux control coefficients extracted from the literature. Blomberg and Adler (1989) determined the apparent flux control coefficient for glycerol-3-phosphate dehydrogenase (Gpd p, reaction 1) as 0.6. This value (denoted as $C_{e_1}^{v_{net}}$) was experimentally estimated in a osmotolerance study of *Saccharomyces cerevisiae*. Given that $C_{e_1}^{v_{net}} = 0.6$ and applying the summation theorem $\sum_i C_{e_i}^{v_{net}} = 1$ (Fell 1997), we estimated the scaled flux control coefficient for glycerol-3-phosphatase $C_{e_2}^{v_{net}}$ as 0.4. Assuming a classic kinetic model, Cronwright et al. (2002) calculated the scaled flux control coefficients during different growth phases of *S. cerevisiae*. The kinetic model incorporates measurements of metabolite concentrations, maximal enzyme rates and kinetic parameters reported in the literature. The scaled flux control coefficients of Blomberg and Adler (1989) and Cronwright et al. (2002) suggest that the glycerol biosynthetic pathway is chiefly controlled by glycerol-3-phosphate dehydrogenase (Gpd p, reaction 1). The importance of glycerol-3-phosphate dehydrogenase on the pathway flux has been frequently reported in the literature (Nevoigt and Stahl 1996; Michnick et al. 1997; Remize et al. 1999; Remize et al. 2001).

In this study, the flux control of the pathway enzymes was assessed by statistically evaluating the computed scaled flux control coefficients. Our MCA procedure assumes no specific knowledge of the enzyme kinetics and the scaled elasticities are obtained by two different sampling approaches [case (i) & (ii)]. We deliberately excluded *a priori* knowledge to evaluate the capability of the methodology and to examine the influence of the enzyme kinetics on the scaled flux control coefficients. Furthermore, our computations of the scaled flux control coefficients require no knowledge of the kinetic parameters but are based on stoichiometry and thermodynamics. The following discussion focuses on the scaled flux control coefficients of glycerol-3-phosphate dehydrogenase (Gpd p, reaction 1, $C_{e_1}^{v_{net}}$). The coefficients of glycerol-3-phosphatase (Gpp p, reaction 2, $C_{e_2}^{v_{net}}$) are then directly obtained from the summation theorem $\sum_i C_{e_i}^{v_{net}} = 1$.

In case (i), the scaled elasticities were uniformly sampled and correlated within defined ranges as described by Steuer et al. (2006) and Grimbs et al. (2007). This approach exploits the fact that, in typical enzyme reactions, the scaled elasticities are confined to specific ranges. Without further information on the scaled elasticities, the system can be most generally examined by uniformly sampling the scaled elasticities within these ranges (Wang et al. 2004). Applying this approach in the present study, the mean and median values of the distributed scaled flux control coefficients for glycerol-3-phosphate dehydrogenase (the $C_{e_1}^{v_{net}}$ distribution) are 0.57 and 0.56, respectively. The 20 % quantile $Q_{0.2}$ is 0.36, indicating that 80 and 20 % of the calculated $C_{e_1}^{v_{net}}$ values are greater and less than 0.36, respectively. The 80 % quantile ($Q_{0.8}$) is 0.79 (i.e. 80 and 20 % of the calculated $C_{e_1}^{v_{net}}$ values are

smaller and greater than 0.79, respectively). This result implies that the glycerol-3-phosphate dehydrogenase has a slightly larger control over the pathway flux compared with the glycerol-3-phosphatase. The calculated mean and median of the distribution of scaled flux control coefficients for glycerol-3-phosphate dehydrogenase are close to the apparent flux control coefficient measured by Blomberg and Adler (1989) (blue star in column 1 of Fig. 4). This result also shows that, within the ensemble of generated states, the pathway flux is not necessarily dominated by the glycerol-3-phosphate dehydrogenase reaction.

In case (ii), the degrees of saturation of active sites were uniformly sampled and combined with scaled elasticity expressions derived from two rate laws based on the convenience rate law (Wang et al. 2004; Liebermeister and Klipp 2006; Chakrabarti et al. 2013). The convenience rate law can be regarded as a general approximation to enzyme kinetic rate laws (Chakrabarti et al. 2013). Furthermore, this generalized rate law is adopted in dynamical models of biochemical reaction networks with plausible biological properties (Liebermeister and Klipp 2006). Using this approach, the mean and median of the distribution of the calculated scaled flux control coefficients for glycerol-3-phosphate dehydrogenase (the $C_{e_1}^{v_{net}}$ distribution) are 0.77 and 0.81, respectively. The $C_{e_1}^{v_{net}}$ distribution is shifted to larger values of scaled flux control coefficients compared with case (i). Specifically, in case (ii), $Q_{0.2} = 0.59$ and $Q_{0.8} = 0.96$. The mean and median of the calculated $C_{e_1}^{v_{net}}$ distribution approach the $C_{e_1}^{v_{net}}$ values determined by Cronwright et al. (2002) (see Fig. 4). The $C_{e_1}^{v_{net}}$ of 0.6 obtained by Blomberg and Adler (1989) is within the 20–80 % quantile range of the present study. Hence, in most of the simulated states, the pathway flux is primarily controlled by glycerol-3-phosphate dehydrogenase. The variation in flux control between cases (i) and (ii) may be attributed to combining the explicit scaled elasticity expressions with uniform sampling of the degrees of saturation of active sites in the latter case. In the kinetic model of Cronwright et al. (2002), the scaled flux control coefficients were evaluated from specific enzyme rate laws. In our study, the scaled elasticity expressions were derived from the convenience rate law, but are generally similar to those of Cronwright et al. (2002). Therefore, in case (ii), our model might yield similar dynamical behavior to Cronwright et al.'s model (2002). Both models suggest a larger flux control of glycerol-3-phosphate dehydrogenase than was obtained by Blomberg and Adler (1989). Moreover, this result suggests that the simulated flux control of the pathway enzymes is sensitive to the details of the enzyme kinetics. A similar result was reported by Wang et al. (2004).

Conclusions

We have performed a coupled thermodynamic and flux control analysis of the glycerol biosynthesis pathway. The methodology was verified on a well-studied biosynthetic pathway; namely, glycerol biosynthesis in *Saccharomyces cerevisiae*. Under the investigated steady-state conditions, glycerol-3-phosphate dehydrogenase was found to operate far from thermodynamic equilibrium. In contrast, glycerol-3-phosphatase can operate near and far from thermodynamic equilibrium, and also at intermediate modes. Our calculated distributions of scaled flux control coefficients, obtained by combining scaled elasticity expressions derived from the convenience rate law with uniform sampling of the degrees of saturation of active sites, demonstrated a similar flux control trend to that reported by Blomberg and Adler (1989) and Cronwright et al. (2002). More precisely, the pathway flux was chiefly governed by glycerol-3-phosphate dehydrogenase.

In summary, the applied approach properly predicted the flux control of glycerol-3-phosphate dehydrogenase without *a priori* knowledge of specific enzyme kinetic rate laws and parameters. The applied approach is instead based on stoichiometry and thermodynamics. Deriving scaled elasticity expressions from the convenience rate law is a promising alternative option for analyzing pathways with unknown enzyme kinetics. The resultant information could improve the experimental design of genetic engineering of metabolic pathways, especially by reducing the development time and the number of experiments. Finally, to fully assess the capability of the proposed methodology, additional investigation of other complex biochemical reaction networks is needed.

Acknowledgments This work was financed by the German Federal Ministry of Education and Research (BMBF) in the

context of the NANOKAT graduate program (ref. no. 0316052A). This study was inspired by interdisciplinary discussions within the graduate program.

Supporting Information Metabolite concentration ranges for the optimization and sampling procedure of $\Delta_r G'$

Calculation of $\Delta_r G_1'^0$ and $\Delta_r G_2'^0$ from literature data

Generating $\Delta_r G_1'$ and $\Delta_r G_2'$ combinations by sampling the metabolite concentrations in logarithmic space

Calculation of scaled elasticity values for determining the scaled flux control coefficients

Calculation of scaled flux control coefficients related to the steady-state net flux

Combinations of thermodynamically feasible disequilibrium ratios ρ_1 and ρ_2 (converted from the $\Delta_r G_1'$ and $\Delta_r G_2'$ values; see Fig. 3 in the main text)

References for Supporting Information

References

Alberty RA, Cornish-Bowden A, Goldberg RN, Hammes GG, Tipton K, Westerhoff HV (2011) Recommendations for terminology and databases for biochemical thermodynamics. Biophys Chem 155:89–103

Albertyn J, van Tonder A, Prior BA (1992) Purification and characterization of glycerol-3-phosphate dehydrogenase of *Saccharomyces cerevisiae*. FEBS Lett 308:130–132

Benham T (2011) Uniform distribution over a convex polytope. MATLAB Central File Exchange. http://www.mathworks.com/matlabcentral/fileexchange/34208-uniform-distribution-over-a-convex-polytope/content/cprnd.m. Accessed 25 September 2013

Blomberg A, Adler L (1989) Roles of glycerol and glycerol-3-phosphate dehydrogenase (NAD^+) in acquired osmotolerance of *Saccharomyces cerevisiae*. J Bacteriol 171:1087–1092

Chakrabarti A, Miskovic L, Soh KC, Hatzimanikatis V (2013) Towards kinetic modeling of genome-scale metabolic networks without sacrificing stoichiometric, thermodynamic and physiological constraints. Biotechnol J 8:1043–1057

Cronwright GR, Rohwer JM, Prior BA (2002) Metabolic control analysis of glycerol synthesis in *Saccharomyces cerevisiae*. Appl Environ Microbiol 68:4448–4456

Cvijovic M, Bordel S, Nielsen J (2011) Mathematical models of cell factories: moving towards the core of industrial biotechnology. Microb Biotechnol 4:572–584

Fell D (1997) Understanding the control of metabolism. Portland Press, London

Goldberg RN, Tewari YB (1994) Thermodynamics of enzyme-catalyzed reactions. part 3. hydrolases. J Phys Chem Ref Data 23:1035–1103

Goldberg RN, Tewari YB, Bell D, Fazio K, Anderson E (1993) Thermodynamics of enzyme-catalyzed reactions. part 1. oxidoreductases. J Phys Chem Ref Data 22:515–582

Grimbs S, Selbig J, Bulik S, Holzhütter HG, Steuer R (2007) The stability and robustness of metabolic states: identifying stabilizing sites in metabolic networks. Mol Syst Biol 3:146. doi:10.1038/msb4100186

Hatzimanikatis V, Floudas CA, Bailey JE (1996) Analysis and design of metabolic reaction networks via mixed-integer linear optimization. AIChE J 42:1277–1292

He W, Ye S, Xue T, Xu S, Li W, Lu J, Cao L, Ye B, Chen Y (2014) Silencing the glycerol-3-phosphate dehydrogenase gene in *Saccharomyces cerevisiae* results in more ethanol being produced and less glycerol. Biotechnol Lett 36:523–529

Heinrich R, Rapoport TA (1974) A linear steady-state treatment of enzymatic chains: general properties, control and effector strength. Eur J Biochem 42:89–95

Hubmann G, Guillouet S, Nevoigt E (2011) Gpd1 and Gpd2 fine-tuning for sustainable reduction of glycerol formation in *Saccharomyces cerevisiae*. Appl Environ Microbiol 77:5857–5867

Kacser H, Burns JA (1973) The control of flux. Symp Soc Exp Biol 27:65–104

Kaufman DE, Smith RL (1998) Direction choice for accelerated convergence in hit-and-run sampling. Oper Res 46:84–95

Klipp E, Liebermeister W, Wierling C (2004) Inferring dynamic properties of biochemical reaction networks from structural knowledge. Genome Inform 15:125–137

Kümmel A, Panke S, Heinemann M (2006) Putative regulatory sites unraveled by network-embedded thermodynamic analysis of metabolome data. Mol Syst Biol. doi:10.1038/msb4100074

Liebermeister W, Klipp E (2006) Bringing metabolic networks to life: convenience rate law and thermodynamic constraints. Theor Biol Med Model 3:41. doi:10.1186/1742-4682-3-41

Michnick S, Roustan JL, Remize F, Barre P, Dequin S (1997) Modulation of glycerol and ethanol yields during alcoholic fermentation in *Saccharomyces cerevisiae* strains overexpressed or disrupted for GPD1 encoding glycerol 3-phosphate dehydrogenase. Yeast 13:783–793

Miskovic L, Hatzimanikatis V (2010) Production of biofuels and biochemicals: in need of an ORACLE. Trends Biotechnol 28:391–397

Murabito E (2013) Targeting breast cancer metabolism: a metabolic control analysis approach. Curr Synthetic Sys Biol 1:104. doi:10.4172/2332-0737.1000104

Murabito E, Smallbone K, Swinton J, Westerhoff HV, Steuer R (2011) A probabilistic approach to identify putative drug targets in biochemical networks. J R Soc Interface 8:880–895

Nevoigt E, Stahl U (1996) Reduced pyruvate decarboxylase and increased glycerol-3-phosphate dehydrogenase [NAD^+] levels enhance glycerol production in *Saccharomyces cerevisiae*. Yeast 12:1331–1337

Ou X, Ji C, Han X, Zhao X, Li X, Mao Y, Wong LL, Bartlam M, Rao Z (2006) Crystal structures of human glycerol 3-phosphate dehydrogenase 1 (GPD1). J Mol Biol 357:858–869

Reder C (1988) Metabolic control theory: a structural approach. J Theor Biol 135:175–201

Remize F, Barnavon L, Dequin S (2001) Glycerol export and glycerol-3-phosphate dehydrogenase, but not glycerol phosphatase, are rate limiting for glycerol production in *Saccharomyces cerevisiae*. Metab Eng 3:301–312

Remize F, Roustan JL, Sablayrolles JM, Barre P, Dequin S (1999) Glycerol overproduction by engineered

Saccharomyces cerevisiae wine yeast strains leads to substantial changes in by-product formation and to a stimulation of fermentation rate in stationary phase. Appl Environ Microbiol 65:143–149

Rolleston FS (1972) A theoretical background to the use of measured concentrations of intermediates in study of the control of intermediary metabolism. Curr Topics Cell Regul 5:47–75

Romero PJ, de Meis L (1989) Role of water in the energy of hydrolysis of phosphoanhydride and phosphoester bonds. J Biol Chem 264:7869–7873

Soh KC, Hatzimanikatis V (2010) Network thermodynamics in the post-genomic era. Curr Opin Microbiol 13:350–357

Soh KC, Miskovic L, Hatzimanikatis V (2012) From network models to network responses: integration of thermodynamic and kinetic properties of yeast genome-scale metabolic networks. FEMS Yeast Res 12:129–143

Steuer R, Gross T, Selbig J, Blasius B (2006) Structural kinetic modeling of metabolic networks. Proc Natl Acad Sci USA 103:11868–11873

Tran LM, Rizk ML, Liao JC (2008) Ensemble modeling of metabolic networks. Biophys J 95:5606–5617

Wang L, Birol İ, Hatzimanikatis V (2004) Metabolic control analysis under uncertainty: framework development and case studies. Biophys J 87:3750–3763

Young HL, Pace N (1958) Some physical and chemical properties of crystalline α-glycerophosphate dehydrogenase. Arch Biochem Biophys 75:125–141